Original Article

Dependence of Hydrothermal Time on Structural Characteristics and Photocatalytic Properties of SnO$_2$ Nanoparticles

Pham Van Tuan[1,*], Le Trung Hieu[1], Vu Thi Tan[2], Hoang Ba Tuong[2], Tran Thi Quynh Hoa[3], Nguyen Xuan Sang[4], Tran Ngoc Khiem[1]

[1]International Training Institute for Materials Science (ITIMS),
Hanoi University of Science and Technology, 1 Dai Co Viet, Hanoi, Vietnam

[2]School of Chemical Engineering, Hanoi University of Science and Technology,
1 Dai Co Viet, Hanoi, Vietnam

[3]Faculty of Mechanical Engineering, National University of Civil Engineering (NUCE),
55 Giai Phong, Hanoi, Vietnam

[4]Department of Electronics and Telecommunications, Saigon University,
273 An Duong Vuong, District 5, Ho Chi Minh City,, Vietnam

Abstract: In this work, SnO$_2$ nanoparticles were prepared by hydrothermal method using SnCl$_4$.5H$_2$O and NaOH at 180 °C for different hydrothermal times. The effect of hydrothermal time on the crystal structure, morphology, chemical bonding, and photocatalytic properties of SnO$_2$ nanoparticles was studied. Structural and morphological characteristics of SnO$_2$ nanoparticles were investigated by X-ray diffraction and electron scanning microscopy analyses. Chemical bonding and absorption properties of the prepared materials were analyzed by Fourier transform infrared spectroscopy and UV-Vis absorption spectroscopy. Photocatalytic properties of SnO$_2$ nanoparticles were evaluated by the degradation of methylene blue dye under visible-light irradiation.

Keywords: SnO$_2$ nanoparticles, hydrothermal time, photocatalytic properties

_____

*Corresponding author.
 Email address: tuan.phamvan@hust.edu.vn

1. Introduction

Organic dyes are widely used in various industries, such as textiles, plastics, paper, cosmetics, leather, food, and pharmaceuticals. These dyes are highly toxic, causing serious human illnesses and affecting the global ecosystem. Therefore, developing suitable methods to treat these industrial wastes is necessary. In recent years, photocatalytic technology with metal oxide semiconductors has been developed as an effective method to address environmental pollution. In semiconductor metal oxides, tin oxide (SnO_2) is considered an effective photocatalytic material [1–3]. SnO_2 has many advantages such as abundant reserve, low cost, non-toxicity, good environmental compatibility, excellent photocatalytic activity, and high chemical stability [4–6]. Moreover, the bandgap of SnO_2 could be varied from Eg = 2.5-3.4 eV, which is suitable to harvest a long range of visible wavelength from sunlight [7]. SnO_2 nanostructures have a large specific surface area that provides high photocatalytic efficiency [8].

Various methods, such as hydrothermal method [8–11], microwave irradiation [12], and green synthesis [7,13], have been developed to synthesize SnO_2 nanostructures. Hydrothermal method is widely used to manufacture highly active SnO_2 photocatalyst nanomaterials [9, 10]. Complex SnO_2 nanoparticles and nanosheets synthesized through hydrothermal process demonstrated excellent photocatalytic activity for rhodamine 6G (R6G) dyes [9]. Meanwhile, flower-like SnO_2 nanostructures synthesized through hydrothermal method showed superior photocatalytic performance in the decomposition of methyl orange (MO) dyes [14]. Moreover, novel hierarchical dahlia-like SnO_2 nanostructures prepared by hydrothermal method exhibited photocatalytic activity to rhodamine B (RhB) aqueous solution [10]. These reports show that SnO_2 nanostructures can be efficiently synthesized by hydrothermal method. However, to the best of our knowledge, no study has investigated the effect of hydrothermal time on the structure, morphology, and photocatalytic properties of SnO_2 nanostructures.

In this study, we report on the fabrication of SnO_2 nanostructures by hydrothermal method and determine the effect of hydrothermal time on structure, morphology, and photocatalytic properties.

2. Experimental

2.1. Materials

Tin (IV) chloride pentahydrate (98%), sodium hydroxide, and ethanol (absolute garde for analysis) were used as precursors for SnO_2 synthesis by hydrothermal method. These chemicals were purchased from Merck and Sigma-Aldrich. All chemicals were used without further purification.

2.2. Synthesis of SnO$_2$ Nanoparticles

SnO_2 nanoparticles were synthesized by hydrothermal method. In typical synthesis, $SnCl_4.5H_2O$ (0.1 g) was dissolved in 30 ml of deionized water by magnetic stirring for 30 minutes. NaOH (0.2 g) was dissolved in 30 ml of deionized water under stirring for 30 minutes. The NaOH solution was slowly added to the $SnCl_4.5H_2O$ solution until the pH reached 7. The mixture was poured into a Teflon autoclave, which was tightened and placed in an oven at room temperature. The hydrothermal temperature of the oven was increased to 180 °C. The hydrothermal duration was varied from 5 to 25 hours. After the hydrothermal process, the oven was naturally cooled to room temperature. The precipitate in the Teflon autoclave was washed with deionized water and ethanol three times. The obtained product was dried at 80 °C for 24 hours.

2.3. Characterization

The crystal structure and phase composition of the synthesized samples were characterized by X-ray diffraction (XRD) analysis using X-ray diffractometry (XRD; Siemens D5000, Germany) with Cu-Kα radiation (λ = 1.5406 Å). The morphological characteristics of the samples were evaluated by field-emission scanning electron microscopy (S-4800 FE-SEM, Hitachi, Japan). Absorption properties were studied by UV-Vis absorption spectrophotometry (V-650 Jasco, USA) within the wavelength range of 200–800 nm. Chemical bonds were analyzed by Fourier transform infrared spectroscopy (IRAffinity-1s, Shimadzu) within 400–4000 cm^{-1}.

2.4. Photocatalytic measurements

The photocatalytic activity of the samples was evaluated by methylene blue (MB) degradation under visible-light irradiation using a standard 60 W filament lamp at a distance of 10 cm. The initial concentration of MB was 1 μg/ml. About 30 mg of the SnO_2 photocatalyst was added to 50 ml of the MB solution. Before light irradiation, the suspension was magnetically stirred in the dark for 60 minutes to reach the adsorption–desorption equilibrium. Every 20 minutes during irradiation, 5 ml of the suspension was collected and centrifuged to measure the remaining MB concentration in the solution. The concentration of the MB solution was determined by measuring the maximum absorbance change through UV-Vis spectrophotometer (V-650 Jasco, USA).

3. Results and Discussion

The X-ray diffraction patterns of SnO_2 nanoparticles fabricated with different hydrothermal times are shown in Figure 1. Diffraction peaks with 2θ values of 27.08°, 34.25°, 38.51°, 52.08°, 54.86°, 61.78°, 65.63°, 71.48°, and 78.65° correspond to the crystal planes (110), (101), (200), (211), (220), (310), (301), (202), and (321), respectively. Based on the standard X-ray diffraction JCPDS No. 41-1445 [13,15–17], the synthesized SnO_2 nanoparticles have a rutile tetragonal crystal structure. As the hydrothermal time increased, the intensity of the diffraction peaks increased due to improvement in the crystalline structure. Diffraction peaks corresponding to other phases were not observed, indicating the high purity of the synthesized samples.
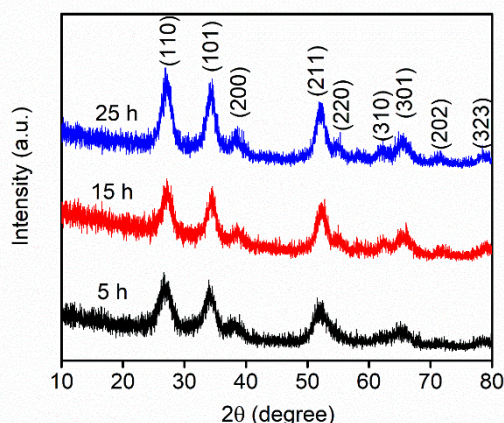
Figure 1. XRD patterns of SnO_2 nanoparticles fabricated using various hydrothermal times.

The crystal size of the SnO_2 nanoparticles was calculated using the Scherrer formula [16,17]: $D = 0.9\,\lambda/(\beta\cos\theta)$, where λ is the X-ray wavelength (1.5406 Å), θ is the Bragg diffraction angle, and β is the full-width half-maximum (FWHM). Table 1 shows the crystal sizes of the SnO_2 nanoparticles fabricated. The crystal sizes were 3.52, 4.95, and 4.78 nm for particles synthesized by hydrothermal method for 5, 15, and 25 hours, respectively. After 25 hours of hydrothermal process, the particle size of the synthesized samples increased slightly to about 3.52–4.78 nm.

Table 1. Dependence of SnO_2 particle size on hydrothermal time.

Samples	Planes	2θ (degree)	FWHM (degree)	Peak Height	Crystal size (nm)	Average crystal size (nm)
SnO_2 (5 h)	(110)	26.83	2.35	44.93	3.63	
	(101)	34.09	2.17	39.77	4.00	3.52
	(211)	52.21	3.15	32.88	2.92	
SnO_2 (15 h)	(110)	27.11	1.77	42.89	4.82	
	(101)	34.37	1.54	42.14	5.64	4.95
	(211)	52.33	2.10	43.07	4.40	
SnO_2 (25 h)	(110)	27.05	1.93	67.36	4.42	
	(101)	34.28	1.63	58.94	5.33	4.78
	(211)	52.16	2.02	51.68	4.58	

Figure 2 shows the FESEM images of SnO_2 nanoparticles fabricated using different hydrothermal times. SnO_2 nanoparticles were spherical and had relatively uniform particle size and narrow particle size distribution of about 4–10 nm. SnO_2 nanoparticles exhibited minor tendency of agglomeration; when the hydrothermal time was increased, SnO_2 nanoparticles tended to separate. Other morphologies such as nanorods and nanoflowers were not observed. The morphology of SnO_2 nanoparticles did not change, and the particle size increased slightly with increasing hydrothermal time. This result agrees with the XRD data, thereby confirming that the morphology and size of the nanomaterials were slightly affected by hydrothermal time.

The FT-IR infrared spectra of the three as-prepared samples are shown in Figure 3. The FT-IR spectra showed a similar band range in the three samples: the peak at 666 cm^{-1} represents the asymmetric stretching vibrations of Sn-O-Sn in SnO_2 [7,13,17], the peak at 1464 cm^{-1} represents the stretching vibrations of Sn-O [13,17], and the peak at 3179 cm^{-1} represents the stretching vibration of O-H [7,13,17–19]. This result demonstrated the formation of tin oxide in the samples. The intensity of the absorption band depends on hydrothermal time. The amount of SnO_2 nanoparticles formed in the sample fabricated with hydrothermal times of 15 and 25 hours was higher than that in the sample obtained by hydrothermal process for 5 hours. Hence, SnO_2 nanoparticles were successfully fabricated by hydrothermal method.

UV-Vis absorption spectroscopy is a powerful non-destructive tool for investigating the optical properties of nanostructures. Figure 4a shows the UV-Vis absorption spectra of SnO_2 samples prepared with different hydrothermal times. The absorption spectra of SnO_2 nanoparticles were recorded within the wavelength range of 250–850 nm. The results indicated a characteristic absorption peak at 300 nm, which could be attributed to SnO_2 nanoparticles [16,18,20].
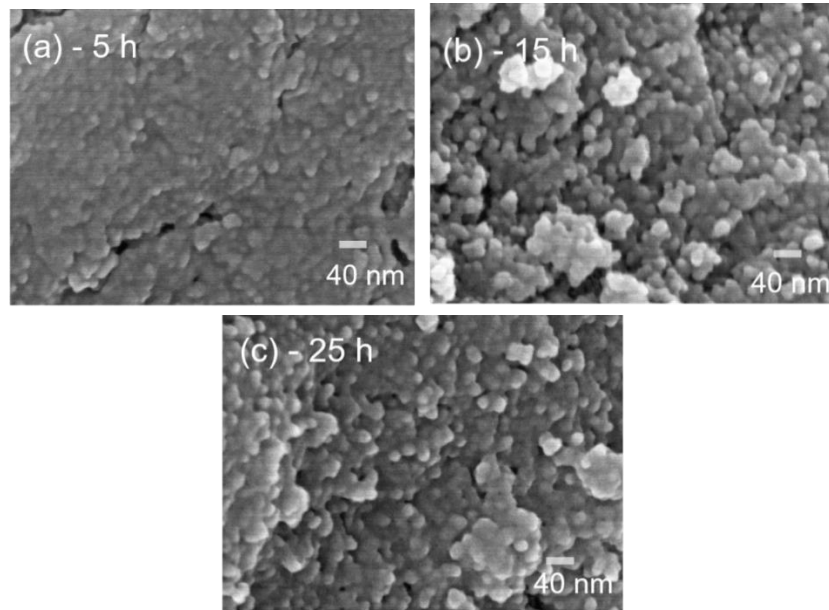
Figure 2. FESEM images of SnO_2 nanoparticles obtained at different hydrothermal times.
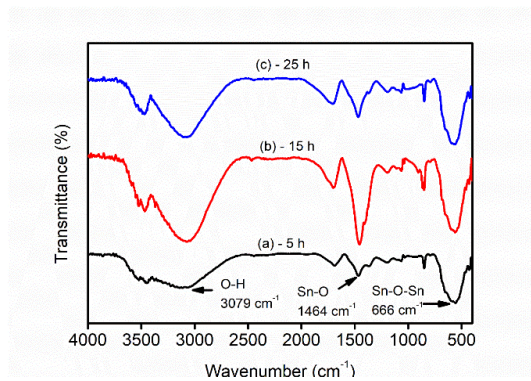
Figure 3. FT-IR spectra of SnO_2 nanoparticles fabricated with different hydrothermal times.
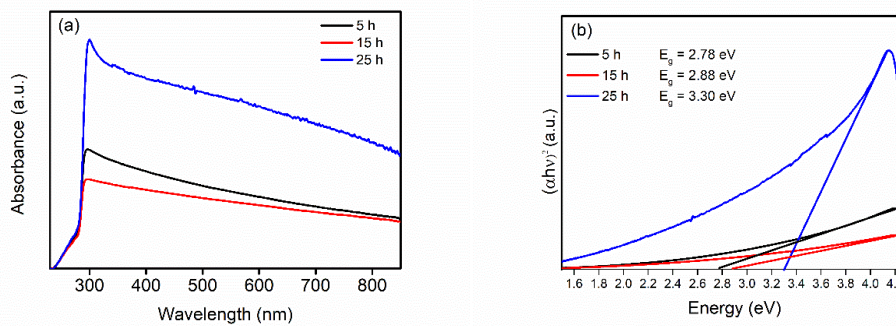
Figure 4. (a) UV-Vis spectra and (b) Tauc's plots of SnO_2 nanoparticles fabricated with different hydrothermal times.

The band gap energy of the samples was calculated from the UV-Vis absorption spectra by using the TAUC model [3]. The model relates the absorption coefficient of the energy of the incident photon by the following equation [13,16]:

$$\alpha(v)hv = K(hv - E_g)^n$$

where $\alpha(v)$ is the absorption coefficient that can be defined according to Beer–Lambert's law, hv is the incident photon energy, E_g is the band gap energy, and K is the constant. The value of n is related to the optical properties of the semiconductor [13,17]. The exponent n of the equation depends on the type of transition and has the values of 1/2, 2, 3/2, and 3 for direct allowed, indirect allowed, direct prohibited, and indirect prohibited transitions, respectively [13,17]. In the case of SnO_2 nanoparticles, the value of n is 1/2 for direct allowed transition [13,16,17]. Figure 4b shows the plot of $(\alpha hv)^2$ versus (hv) for the samples fabricated with hydrothermal times of 5, 15, and 25 hours. Hence, the band gap energy of the SnO_2 semiconductor can be obtained from the plot $(\alpha hv)^2$ as a function of optical energy (E) by extrapolating the linear parts of the graph intersecting the photon energy axis [16,17]. The E_g values of the samples were 2.78, 2.88, and 3.30 eV, respectively. The band gap increased with increasing hydrothermal time. The increase in band gap energy can be due to the decrease in the defective energy levels produced in the band gap of SnO_2 as the hydrothermal time increases.

The photocatalytic activity of SnO_2 nanoparticles was examined by MB dye degradation. Figure 5 shows photocatalytic decomposition based on the absorption spectra of MB in visible light over a period
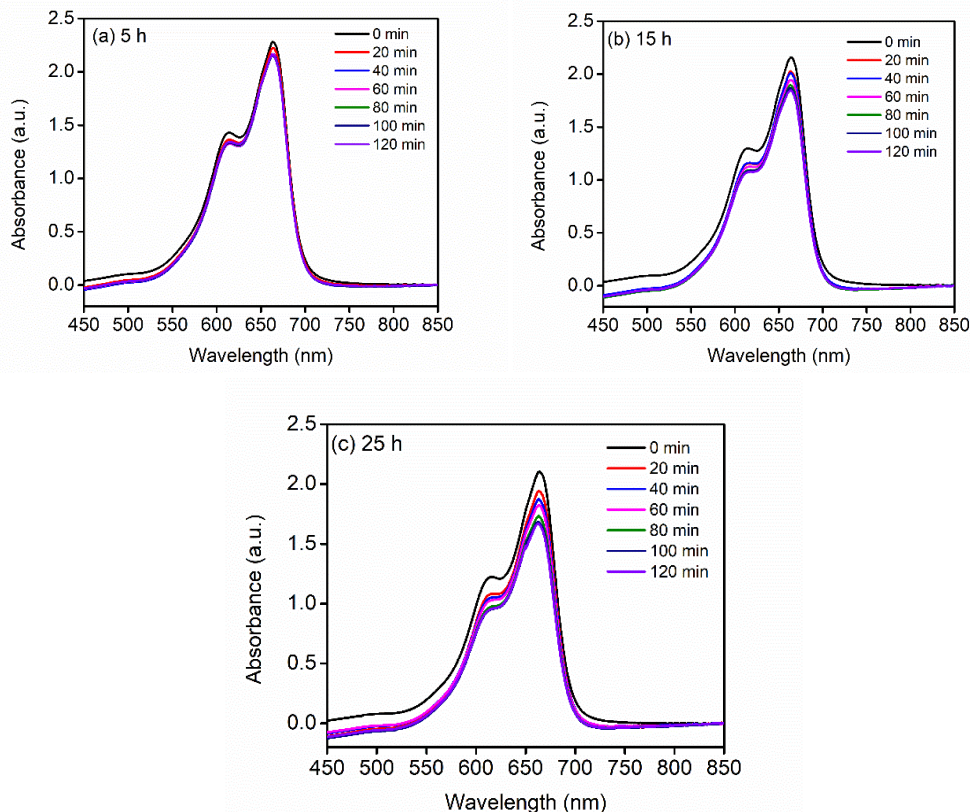
Figure 5. Time-dependent photodegradation absorption spectra of MB dye in the presence of SnO_2 nanoparticles prepared with various hydrothermal times.

of 0 to 120 minutes. The absorption peak of MB at 665 nm [12] was demonstrated in all samples, and the intensity of this absorption peak decreased slightly over time until the final illumination time of 120 min. The light decrease could be because SnO_2 nanomaterials negligibly absorb visible light.

The photocatalytic performance of SnO_2 samples is presented in Figure 6 for detailed study of photocatalytic activity. The concentrations of MB decreased by 6%, 14%, and 17% in samples prepared with hydrothermal times of 5, 15, and 25 hours after 120 minutes of light irradiation. The sample prepared by 25 h of hydrothermal method exhibited the highest photocatalytic capacity.
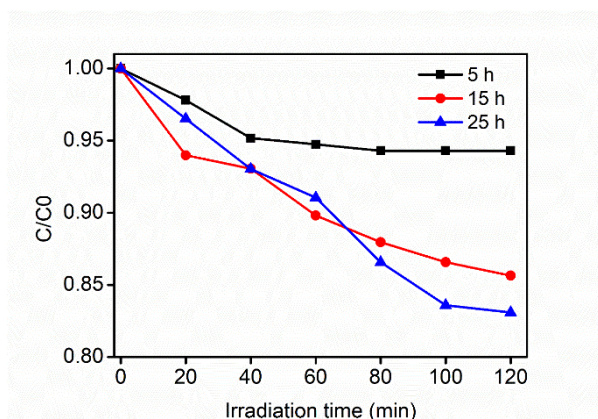
Figure 6. Photocatalytic performance of SnO_2 nanoparticles prepared with various hydrothermal times.

The photocatalytic mechanism of SnO_2 nanoparticles is explained as follows: before the photocatalytic decomposition, MB molecules are absorbed on the surface of SnO_2 nanoparticles [13]. This absorption is due to the charge difference between the negatively charged SnO_2 nanoparticles and the positively charged MB molecules [13]. The photocatalytic degradation of MB begins when the SnO_2 catalyst is exposed to visible light. Electrons in the valence band are excited and jump on the conduction band of SnO_2 and create hole–electron pairs [9,10,13,16]. The holes in the valence band react with water molecules (H_2O) to form hydroxyl radical (OH^-), and conduction band electrons react with dissolved oxygen in the water to form superoxide radical (O_2*) [9,10,13,16]. The two radicals are strongly oxidized, allowing them to react with MB molecules and leading to the efficient decomposition of MB and production of water (H_2O) and carbon dioxide (CO_2) [4,9,13].

4. Conclusion

In this study, SnO_2 nanoparticles were successfully fabricated by hydrothermal method at different synthesis times. The crystal structure and morphology of SnO_2 slightly changed when the hydrothermal time was increased. The crystallinity of SnO_2 nanoparticles also notably increased. The photocatalytic properties of SnO_2 nanoparticles increased with increasing hydrothermal time due to the change in the band gap and crystallization of SnO_2.

Acknowledgments

References

[1] G. Elango, S. M. Roopan, Efficacy of SnO_2 Nanoparticles Toward Photocatalytic Degradation of Methylene Blue Dye, J. Photochem. Photobiol. B Biol, Vol. 155, 2016, pp. 34-38, https://doi.org/10.1016/j.jphotobiol.2015.12.010.

[2] K. Prakash, P. S. Kumar, S. Pandiaraj, K. Saravanakumar, S. Karuthapandian, Controllable Synthesis of SnO_2 Photocatalyst with Superior Photocatalytic Activity for the Degradation of Methylene Blue Dye Solution, J. Exp. Nanosci, Vol. 11, Issue 14, 2016, pp. 1138-1155, https://doi.org/10.1080/17458080.2016.1188222.

[3] A. Bhattacharjee, M. Ahmaruzzaman, T. B. Devi, J. Nath, Photodegradation of Methyl Violet 6B and Methylene Blue using Tin-oxide Nanoparticles (Synthesized via a Green Route), J. Photochem. Photobiol., A Chem, Vol. 325, 2016, pp. 116-124, https://doi.org/10.1016/j.jphotochem.2016.03.032.

[4] S. K. Tammina, B. K. Mandal, N. K. Kadiyala, Photocatalytic Degradation of Methylene Blue Dye by Nonconventional Synthesized SnO_2 Nanoparticles, Environ. Nanotechnology, Monit. Manag, Vol. 10, 2018, pp. 339-350, https://doi.org/10.1016/j.enmm.2018.07.006.

[5] Y. Li, Q. Yang, Z. Wang, G. Wang, B. Zhang, Q. Zhang, D. Yang, Rapid Fabrication of SnO_2 Nanoparticle Photocatalyst: Computational Understanding and Photocatalytic Degradation of Organic Dye, Inorg. Chem. Front, Vol. 5, Issue 12, 2018, pp. 3005–3014, https://doi.org/10.1039/C8QI00688A.

[6] B. Esen, T. Yumak, A. Sınağ, T. Yıldız, Investigation of Photocatalytic Effect of SnO_2 Nanoparticles Synthesized by Hydrothermal Method on the Decolorization of Two Organic Dyes, Photochem. Photobiol, Vol. 87, Issue 2, 2011, pp. 267–274, https://doi.org/10.1111/j.1751-1097.2010.00863.x.

[7] J. Ebrahimian, M. Mohsennia, M. Khayatkashani, Photocatalytic-degradation of Organic Dye and Removal of Heavy Metal Ions using Synthesized SnO_2 Nanoparticles by Vitex Agnus-castus Fruit via a Green Route, Mater. Lett, Vol. 263, 2020, pp. 127255. https://doi.org/10.1016/j.matlet.2019.127255.

[8] X. Han, J. Zhao, L. An, Z. Li, Y. Xin, One-step Synthesis of Oxygen Vacancy-rich SnO_2 Quantum Dots with Ultrahigh Visible-light Photocatalytic Activity, Mater. Res. Bull, Vol. 118, 2019, pp. 110486, https://doi.org/10.1016/j.materresbull.2019.05.011.

[9] Y. C. Chang, J. C. Lin, S. Y. Chen, L. Y. Hung, Y. R. Lin, C. Y. Chen, Complex SnO_2 Nanoparticles and Nanosheets with Enhanced Visible-light Photocatalytic Activity, Mater. Res. Bull, Vol. 100, 2018, pp. 429–433, https://doi.org/10.1016/j.materresbull.2018.01.006.

[10] X. Chen, D. Chu, L. Wang, W. Hu, H. Yang, J. Sun, S. Zhu, G. Wang, J. Tao, S. Zhang, Surfactant-free Synthesis of Novel Hierarchical Dahlia-like SnO_2 Nanostructures with Enhanced Visible-light-driven Photocatalytic Activity, J. Alloys Compd, Vol. 768, 2018, pp. 517–524, https://doi.org/10.1016/j.jallcom.2018.06.274.

[11] P. Dammala, J. Machado, B. Rani, S. Murali, S. Devi, M. N. Luwang, N.K. Sahu, Synthesis of Biphasic Nanomaterials Based on ZnO and SnO_2 : Application towards Photocatalytic Degradation of Acid Red Dye, Nano-Structures and Nano-Objects, Vol. 18, 2019, pp. 100292, https://doi.org/10.1016/j.nanoso.2019.100292.

[12] A. Kar, J. Olszówka, S. Sain, S. R. I. Sloman, O. Montes, A. Fernández, S. K. Pradhan, A. E. H. Wheatley, Morphological Effects on the Photocatalytic Properties of SnO_2 Nanostructures, J. Alloys Compd, Vol. 810, 2019, pp. 151718, https://doi.org/10.1016/j.jallcom.2019.151718.

[13] P. A. Luque, O. Nava, C. A. Soto-Robles, M. J. Chinchillas-Chinchillas, H. E. Garrafa-Galvez, Y.A . Baez-Lopez, K. P. Valdez-Núñez, A. R. Vilchis-Nestor, A. Castro-Beltrán, Improved Photocatalytic Efficiency of SnO_2 Nanoparticles through Green Synthesis, Optik (Stuttg), Vol. 206, 2020, pp. 164299, https://doi.org/10.1016/j.ijleo.2020.164299.

[14] J. Wang, H. Fan, H. Yu, Synthesis of Hierarchical Flower-like SnO_2 Nanostructures and Their Photocatalytic Properties, Optik (Stuttg). Vol. 127, Issue 2, 2016, pp. 580–584, https://doi.org/10.1016/j.ijleo.2015.10.104.

[15] Y. MAKINOSE, D. ASAKURA, H. MATSUDA, E. HOSONO, Synthesis of Core-sheath Structured Fibers of SnO_2/carbon Composites by Electrospinning, J. Ceram. Soc. Japan, Vol. 126, 2018, pp. 662-666, https://doi.org/10.2109/jcersj2.18037.

[16] S. Begum, M. Ahmaruzzaman, CTAB and SDS Assisted Facile Fabrication of SnO_2 Nanoparticles for Effective Degradation of Carbamazepine from Aqueous Phase: A Systematic and Comparative study of their Degradation Performance, Water Res, Vol. 129, 2018, pp. 470–485, https://doi.org/10.1016/j.watres.2017.11.031.

[17] H. Mahmood, M. A. Khan, B. Mohuddin, T. Iqbal, Solution-phase Growth of Tin Oxide (SnO_2) Nanostructures: Structural, Optical and Photocatalytic properties, Mater. Sci. Eng. B Solid-State Mater. Adv. Technol, Vol. 258, 2020, pp. 114568, https://doi.org/10.1016/j.mseb.2020.114568.

[18] V. K. Vidhu, D. Philip, Biogenic Synthesis of SnO_2 Nanoparticles: Evaluation of Antibacterial and Antioxidant Activities, Spectrochim. Acta - Part A Mol. Biomol. Spectrosc, Vol. 134, 2015, pp. 372–379, https://doi.org/10.1016/j.saa.2014.06.131.

[19] A. Bhattacharjee, M. Ahmaruzzaman, A Green Approach for the Synthesis of SnO_2 Nanoparticles and its Application in the Reduction of P-nitrophenol, Mater. Lett, Vol. 157, 2015, pp. 260–264, https://doi.org/10.1016/j.matlet.2015.05.053.

[20] X. Han, J. Zhao, L. An, Z. Li, Y. Xin, One-step Synthesis of Oxygen Vacancy-rich SnO_2 Quantum Dots with Ultrahigh Visible-light Photocatalytic Activity, Mater. Res. Bull, Vol. 118, 2019, pp. 110486, https://doi.org/10.1016/j.materresbull.2019.05.011.

[21] N. X. Sang, V. C. Minh, Thermal Annealing-induced Self-junction of Hydrothermal Titanate Nanotubes/TiO_2 Nanoparticles with Enhanced Photocatalytic Activity, Nanotechnology. Vol. 31, No. 43, 2020, pp. 435703, https://doi.org/10.1088/1361-6528/aba65c.